THE JOURNAL OF PHYSICAL CHEMISTRY LETTERS
A JOURNAL OF THE AMERICAN CHEMICAL SOCIETY

pubs.acs.org/JPCL

Letter

Nonequilibrium Lattice Dynamics of Individual and Attached PbSe Quantum Dots under Photoexcitation

Luye Yue, Jingjun Li, Changyuan Yao, Jie Chen, Chang Yan,* Xuan Wang,* and Jianming Cao*

Cite This: *J. Phys. Chem. Lett.* 2024, 15, 7667−7673

Read Online

ACCESS | Metrics & More | Article Recommendations | Supporting Information

ABSTRACT: Quantum dot (QD) solids are emerging materials for many optoelectronic applications. To enhance interdot coupling and charge transport, surface ligands can be removed, allowing individual QDs to be attached along specific crystal orientations (termed "oriented attachment"). Optimizing the electronic and optical properties of QD solids demands a comprehensive understanding of the nanoscale energy flow in individual and attached QDs under photoexcitation. In this work, we employed ultrafast electron diffraction to directly measure how oriented attachment along ⟨100⟩ directions affects the nonequilibrium lattice dynamics of lead selenide QDs. The oriented attachment anisotropically alters the ultrafast energy relaxation along specific crystal axes. Along the ⟨100⟩ directions, both the lattice deformation and atomistic random motions are suppressed in comparison with those of individual QDs. Conversely, the effects are enhanced along the unattached ⟨111⟩ directions due to ligand removal. The oriented attachment switches the major lattice thermalization pathways from ⟨100⟩ to ⟨111⟩ directions.

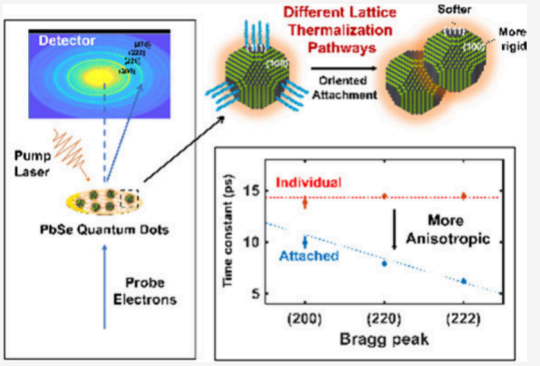

Colloidal semiconductor quantum dots (QDs) have found versatile applications for an array of optoelectronics, because of their affordable production, solution processability, and tunable optical properties.[1−7] An important strategy for achieving the optical benefits of QDs while maintaining good electric transport of bulk materials is the attachment of individual QDs along specific crystal orientations to form electronically coupled QDs.[8−13] Moreover, these QD solids demonstrate intriguing characteristics, including Dirac cones and topological states, thereby holding significant potential for the development of unconventional optoelectronic devices.[14,15]

The device performance of QD-based optoelectronics is fundamentally dependent on the nanoscale energy relaxation pathways of QD building blocks. Following photoexcitation, a significant part of the energy of hot carriers dissipates to the lattice via electron−phonon (E−P) coupling and subsequent phonon−phonon (P−P) coupling. In bulk materials, these energy transfer pathways are mainly governed by the distribution of carrier electronic states, the strength of E−P coupling, and phonon dispersion.[16−18] However, surface effects become significant in QDs due to the high surface:volume ratio of nanocrystals.[19,20] For example, QDs generally exhibit surface-mediated hot carrier dynamics, resulting in a faster carrier cooling rate in smaller dots.[21,22] Also, surface phonon modes are usually softer than the bulk modes, leading to stronger E−P coupling.[23] The oriented attachment can alter surface conditions by shrinking the exposure of certain facets, reducing ligand coverage[24,25] and introducing defects[26] into individual QDs. Consequently, oriented attachment can significantly alter the lattice thermalization pathways, including the E−P and P−P coupling processes.

Optical methods have been used to resolve the excitonic dynamics in QD solids, such as surface trapping of charge carriers[27−29] and enhanced diffusivity of excitons, within the first few hundreds of femtoseconds following photoexcitation.[30,31] When excitons are trapped at the surface, there is a large change in the LO phonon coupling as one can see in the photoluminescence (PL) spectra.[32−35] While optical probing has provided valuable insights into the excitonic dynamics, ultrafast electron diffraction (UED) can yield direct information about the nonequilibrium lattice dynamics by tracking the associated changes in the diffraction pattern using femtosecond electron pulses.[36−40] The lattice dynamics revealed by UED experiments are critical for understanding E−P and P−P coupling in photoexcited QDs.[41−44] UED also has the unique capacity to resolve lattice dynamics along specific crystal orientations and quantify dynamical anisotropy. Recently, UED experiments were used to detect anomalous intensity variations in high-order peaks in CdSe/CdS and PbS

Received: May 25, 2024
Revised: July 15, 2024
Accepted: July 17, 2024
Published: July 22, 2024

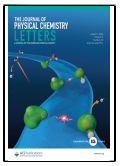

https://doi.org/10.1021/acs.jpclett.4c01541
J. Phys. Chem. Lett. 2024, 15, 7667−7673

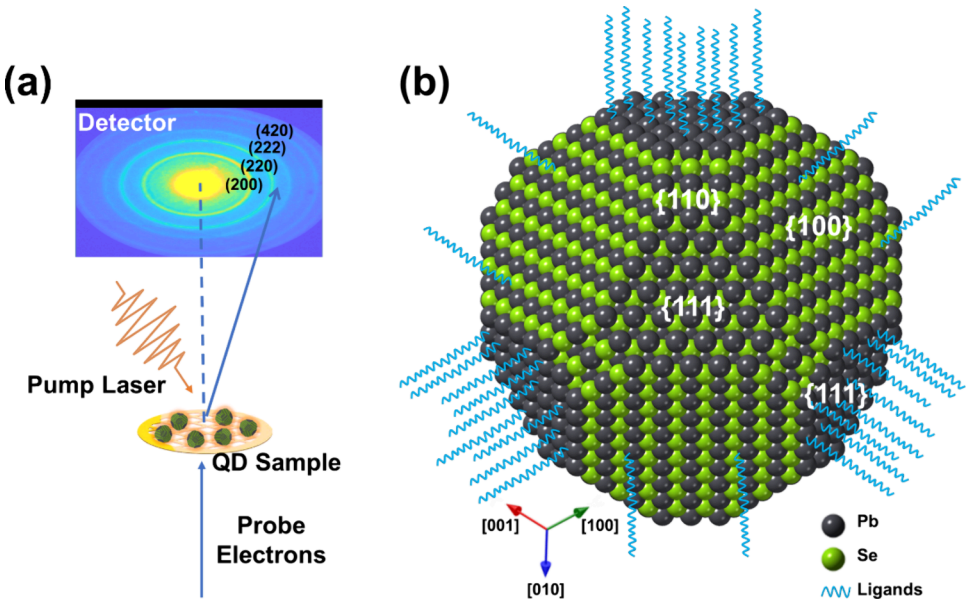

Figure 1. (a) Scheme of the UED experiment in which a femtosecond laser pulse excites PbSe QDs and a 50 kV electron pulse probes the subsequent lattice dynamics. (b) Illustration of a 6 nm PbSe QD with a rock-salt structure, viewed along the <111> direction. Lead and selenium atoms are represented by black and green spheres, respectively. The PbSe QD surface primarily consists of {111} and {100} facets. The blue wavy lines represent surface ligands such as oleic acid and oleyl amine molecules.

QDs, particularly the (400) peak.[45,46] It has also been applied to examine the effects of surface ligands on carrier cooling rates in nanocrystals.[47]

Currently, there is a lack of UED measurements on attached QDs. In this study, we investigate and compare the photoinduced nonequilibrium lattice dynamics in individual and attached PbSe QDs. It is revealed that oriented attachment leads to anisotropic lattice responses along different crystal axes, including lattice expansion, atom mean-square displacement, and lattice thermalization rate. Upon comparison of attached QDs to individual QDs, lattice thermalization was found to be enhanced along ⟨111⟩ directions yet suppressed along ⟨100⟩ directions. Such changes in lattice thermalization pathways can be attributed to the effects of ligand removal and the rigidity difference between the attached {100} facets and the exposed {100} facets. This study advances our understanding of anisotropic nanoscale energy pathways and nonradiative charge recombination in QD solids and devices.

The UED configuration is illustrated in Figure 1a, with further details provided in the Supporting Information. PbSe QDs drop-casted onto a standard transmission electron microscopy (TEM) substrate were excited by an optical pulse (50 fs, 800 nm, 1 kHz repetition rate) followed by an electron pulse, which probes the subsequent lattice dynamics. The PbSe QD samples passivated with ligand molecules such as oleic acids and oleyl amines were synthesized using conventional methods.[48,49] Small PbSe QDs (3−8 nm in diameter) typically display a tetradecahedral structure with {111} and {100} surface facets,[50,51] as depicted in Figure 1b. The ligand coverage of {111} polar facets is higher than that of the {100} and {110} facets due to the favored binding of oleate groups to Pb atoms.[24,52]

As shown in the TEM image in Figure 2a and Figure S3, the diameter of the synthesized QDs is 5.5 ± 0.6 nm, and they are distributed over ∼60% of the substrate, primarily in a single layer. The QD array formed by oriented attachment was prepared by treating the QD layer with a polar solvent, *N*,*N*-dimethylformamide (DMF), to detach surface ligands. The oriented attachment was confirmed by the TEM image in Figure 2b, which showed that QDs are fully attached with no gap between them. The low-magnification TEM images confirmed the attachment of the majority of the QDs (Figure

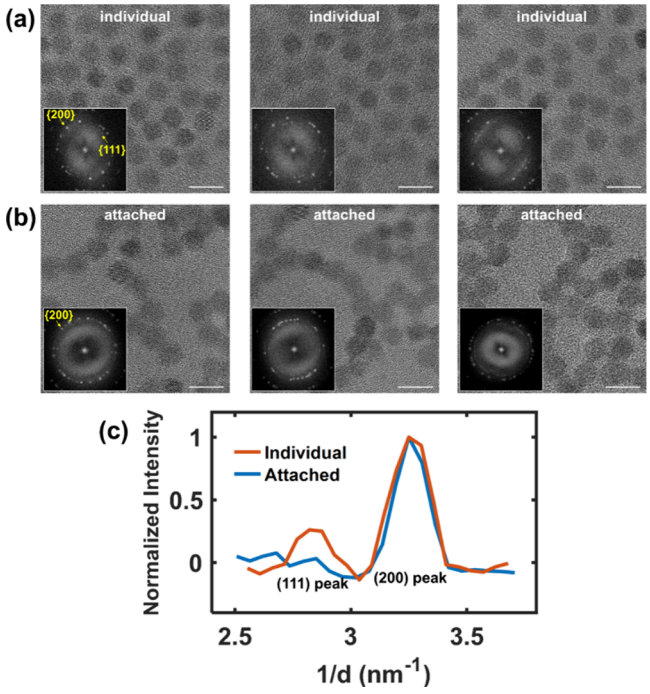

Figure 2. TEM images and corresponding Fourier analysis (insets in the bottom left corners) of the QD (a) before and (b) after DMF treatment, and (c) radial-integrated Fourier-transformed image intensity. The Fourier-transformed image intensities are normalized to the (200) *d* spacing peak for comparison. The attached QDs exhibit a negligible intensity of the (111) peak compared to individual QDs, confirming that DMF treatment induces an oriented attachment along ⟨100⟩ directions. The scale bars in panels a and b are 10 nm.

https://doi.org/10.1021/acs.jpclett.4c01541
J. Phys. Chem. Lett. 2024, 15, 7667−7673

S2). Prior studies have suggested DMF treatment causes a faster removal of ligands on {111} facets than on {100} facets.[53−55] The QDs preferentially orient along the ⟨100⟩ zone axis after the attachment,[25,56,57] as indicated by the disappearance of the {111} d spacing peak in the Fourier transform of TEM images in Figure 2c. The diffraction intensity ratio among the peaks in Figure S6 also confirms the oriented attachment of our QD samples. No change in crystal structure was revealed for the attached QDs by selected area diffraction (SAD) measurements, as indicated by the overlap in lattice constants obtained from various Bragg peaks (Table S1).

The PbSe QDs, with and without DMF treatment (termed individual and attached QDs, respectively), were transferred to a high-vacuum chamber for UED experiments conducted at a base temperature of 90 K. Figure S7 presents a differential UED pattern obtained by subtracting the pattern after time zero from the pattern before time zero. Following photoexcitation, the expansion of interplanar distances causes the diffraction ring to shrink, while enhanced random atomic motion results in an overall decrease in ring intensity. Figure 3

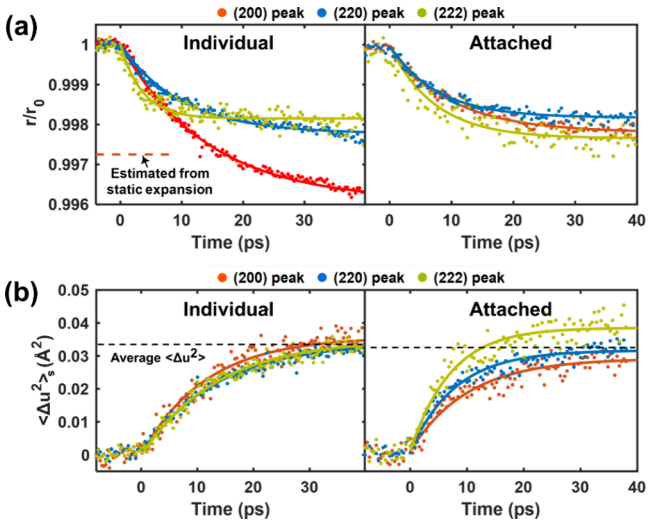

Figure 3. Temporal evolution of (a) normalized Bragg peak positions and (b) atom MSD changes of individual QDs (left) and attached QDs (right) under a pump fluence of 3.6 mJ/cm^2. Different colors represent different Bragg peaks. Solid lines are single-exponential fitting results. In panel a, the Bragg peak positions are normalized to the average value before time zero. The dashed orange line in panel a indicates the estimated (200) peak position variation using the expansion coefficient measured from static measurements. In panel b, the black dashed lines are average values of ⟨Δu^2⟩ among all of the peaks.

presents the time-dependent dynamics of diffraction position, which represents transient lattice expansion. Due to E−P coupling and Auger recombination,[58] the excitons undergo efficient annihilation on a time scale of picoseconds.[20,59] As a result, the lattice temperature increases transiently. The photoexcitation fluence is 3.6 mJ/cm^2, generating ∼50 excitons per dot, and the lattice temperature increases by ∼150 K (details in the Experimental Section in the Supporting Information).

The rock-salt unit cell of bulk PbSe is expected to exhibit isotropic thermal expansion.[60] However, in both types of QDs, we observed an ultrafast anisotropic lattice expansion by measuring the shift of each diffraction peak position. It should be pointed out that the anisotropic thermal expansion of the lattice exists in individual QDs even under static heating conditions (see Figure S4), but the lattice expansion induced by optical excitation under the nonequilibrium conditions deviates significantly from that estimated from static heating conditions. As marked in the left panel of Figure 3a, the corresponding thermal expansion amplitude along ⟨100⟩ directions, measured from the shift of the (200) peak, is ∼20% less under the static condition than under the nonequilibrium condition. This suggests that the system required significantly more time to reach the final equilibrium state than the 40 ps temporal window of UED observation here.

The left panel of Figure 3a clearly shows that the lattice expansion along the ⟨100⟩ directions is more significant than the expansion measured from other peaks. A non-uniform surface ligand distribution on the QD surface could induce asymmetric strain, affecting ultrafast lattice expansion.[61] Surface ligands can exert a dragging force or steric hindrance to limit the physical motion of the lead and selenium atoms on the QD surface. Because the coverage of surface ligands on {100} surface facets is lower than that of {111} surface facets,[24,62] the thermal expansion along the ⟨100⟩ directions is more pronounced than that along the ⟨111⟩ directions.

After oriented attachment, the amplitude of lattice expansion shows different trends among peaks. The expansion amplitude increases along ⟨111⟩ directions and decreases along ⟨110⟩ and ⟨100⟩ directions. The increment of expansion amplitude along the ⟨111⟩ directions can be understood as the consequence of ligand removal during the attachment processes, which loosens the ligands' steric effect and dragging force on surface facets. On the contrary, the obvious suppression of expansion along the ⟨100⟩ directions can be attributed to the oriented attachment on {100} facets. The attachment largely eliminates surface exposure of {100} facets, reducing the surface contribution to the thermal expansion. For the individual PbSe QDs investigated here, the surface atoms, which are softer than those in the QD core,[23,63] comprise approximately half of the total number of atoms. If we consider the combined effects of multiple atomic layers within the surface, rather than just the outermost layer that causes the observed effects, this percentage would be even higher. As a result, the reduction of the surface contribution leads to a reduction of the thermal expansion. The decrease of expansion along the ⟨110⟩ directions might be attributed to the adjacency of {110} facets to the constrained {100} facets.

Further insights into the QD lattice response after photoexcitation were obtained by examining ultrafast changes in the peak width (Figure S8). The broadening of diffraction peaks upon photoexcitation was observed, implying an increased lattice inhomogeneity and embedded strain.[64] It was observed that the broadening of the {200} peak following lattice thermalization in the attached QDs is smaller than that in individual QDs, which aligns well with the enhanced lattice rigidity along the ⟨100⟩ direction. On the contrary, the lack of a stabilizing influence from ligands on the {111} facets results in slightly enhanced broadening of the (222) peak for attached QDs compared to individual QDs.

The dynamics of diffraction peak intensity reveal variations in the random motion of atoms, described by the transient atom mean-square displacement (MSD) ⟨$u(t)^2$⟩ in Figure 3b. Considering that no difference in lattice constants was

https://doi.org/10.1021/acs.jpclett.4c01541
J. Phys. Chem. Lett. 2024, 15, 7667−7673

observed from different SAD peaks (Table S1), we used a harmonic approximation for the atom MSD. The absolute change in peak intensities follows the Debye−Waller effect:

$$I(t) = I_0 \exp[-4\pi^2 \langle \Delta u(t)^2 \rangle_s s^2] \quad (1)$$

where $I(t)$ represents the peak intensity at time t after photoexcitation and I_0 is the peak intensity before photoexcitation. $\langle \Delta u(t)^2 \rangle_s$ is the change of the atom MSD along the corresponding crystal orientation defined by scattering vector s. In the first-order approximation, the averaged $\langle \Delta u(t)^2 \rangle_s$ through all directions is proportional to the lattice temperature change. Figure 3b displays the temporal evolution of $\langle \Delta u(t)^2 \rangle_s$ for individual (left panel) and attached (right panel) QDs. The averaged $\langle \Delta u(t)^2 \rangle_s$ for the three major diffraction peaks is nearly identical for both types of QDs when the lattice reaches a quasi-equilibrium state at 40 ps, as shown by the two well-aligned black dashed lines in Figure 3b. This indicates that the overall temperature increase is similar, which is expected because the excitation fluence was the same for both types of QDs, assuming they have similar absorption coefficients. However, the anisotropy of the atom MSD distributed along specific crystal axes differs between individual and attached QDs. For individual QDs, the $\langle \Delta u(t)^2 \rangle_s$ values for all of the observed peaks exhibit negligible anisotropy, while for attached QDs, $\langle \Delta u(t)^2 \rangle_s$ increases for the (222) peak but decreases for the (200) peak compared to that of individual QDs. This anisotropic trend in $\langle \Delta u(t)^2 \rangle_s$ began after time zero and persisted beyond 40 ps even when the lattice reached a quasi-equilibrium state (see Figure 3b).

The trends in $\langle \Delta u(t)^2 \rangle_s$ for attached and individual QDs across various surface facets are summarized in Figure 4a. While the trend for individual QDs remains relatively flat, a notable slope is observed for attached QDs. The anisotropic trend of $\langle \Delta u(t)^2 \rangle_s$ of attached QDs under photoexcitation is consistent with the anisotropy observed in ultrafast lattice expansion. In attached QDs, the lattice thermalization pathway is changed, leading to increased thermal expansion and thermal random motion along ⟨111⟩ directions and a reduction along ⟨100⟩ directions. Given that the surface atoms comprise approximately half of the total number of atoms, alternation in surface structure could significantly impact the photoexcited dynamics of the entire QD lattice.

To extract the lattice relaxation time constants, we utilized a single-exponential function to fit both peak position and $\langle \Delta u(t)^2 \rangle_s$ data, as shown by the solid lines in panels a and b of Figure 3. The time constants for peak intensity changes are presented in Figure 4b and Figure S11, while those for peak positions are illustrated in Figure S12. Both sets show a similar pattern. The average time constant for attached QDs was smaller and exhibited a more pronounced anisotropy among different diffraction peaks compared to that of individual QDs. This kinetic information on lattice thermalization and phonon dephasing processes offers a valuable understanding of E−P and P−P coupling mechanisms.

The accelerated overall lattice relaxation time of attached QDs can be in part attributed to enhanced E−P coupling by reducing the quantum confinement effect and forming less discrete electronic states.[65] This observation is consistent with the report that photogenerated hot carriers cool more quickly in strongly coupled PbSe QDs than in dispersed QDs.[66] In addition, the ligand removal could induce surface defects, thereby accelerating carrier cooling by introducing additional

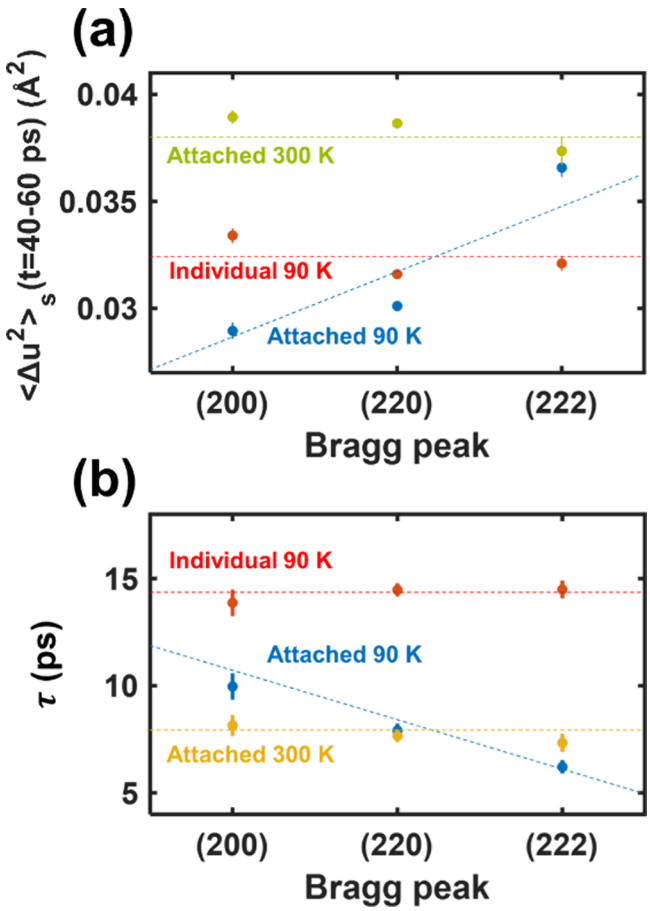

Figure 4. (a) $\langle \Delta u(t)^2 \rangle_s$ in the quasi-equilibrium state (t = 40−60 ps) and (b) time constants (τ) derived from Bragg peak intensity dynamics at a pump fluence of 3.6 mJ/cm^2. Blue, red, and green dots represent the data from attached QDs at 90 K, individual QDs at 90 K, and attached QDs at 300 K, respectively. Error bars indicate one standard deviation. The dashed curves serve as guides for the eye.

energy levels that accelerates phonon dephasing on QD surfaces.[23]

The anisotropy observed in lattice thermalization time constants in attached QDs correlates with the $\langle \Delta u(t)^2 \rangle_s$ data observed in the quasi-equilibrium state (t = 40−60 ps). Diffraction peaks exhibiting larger $\langle \Delta u(t)^2 \rangle_s$ values demonstrate faster lattice thermalization rates, which are evident from the inverse slopes of the blue dashed lines in panels a and b of Figure 4. This distinctive anisotropic lattice relaxation time can be further understood by considering the surface structure alternations. Compared with {100} facets, {111} surface facets are more flexible and have an increased number of surface defects due to ligand removal. Previous studies have indicated that a deficiency in ligands results in off-stoichiometry in Pb and Se atoms, leading to extra surface defect states.[67] These surface defects can induce additional energy levels and cause a broadening of the bandwidth of phonon modes.[23] Consequently, the phonon dephasing time is accelerated along ⟨111⟩ directions, facilitating nanoscale energy transfer within attached dots that is more anisotropic compared to that in individual dots.

The Debye temperature of the 6 nm PbSe QDs is reported to be ∼250 K.[68] As a result, increasing the sample base temperature from 90 to 300 K allows for population of nearly the entire spectrum of phonon modes, encompassing both bulk

https://doi.org/10.1021/acs.jpclett.4c01541
J. Phys. Chem. Lett. 2024, 15, 7667−7673

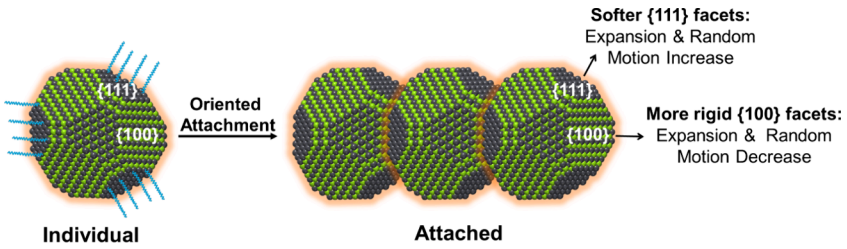

Figure 5. Schematic showing the effect of oriented attachment on the anisotropic response of the PbSe QD lattice under photoexcitation. The surface area along ⟨100⟩ directions decreases, resulting in both an reduced expansion and atom MSD along ⟨100⟩ directions, yet an increased change along ⟨111⟩ directions.

and surface modes, which would smear out the anisotropy of photoinduced lattice dynamics in attached QDs, as shown in Figure 4a. Likewise, similar to the trend observed in atom MSD amplitudes, increasing the QD temperature to 300 K or increasing the pump fluence smears out the anisotropy of lattice thermalization constants, as shown in Figure 4b and Figure S11, respectively. Therefore, the thermal excitation of phonon modes throughout the QD lattice can mitigate the surface effects that cause anisotropic energy flow in attached QDs.

In summary, we investigated the impacts of surface effects on nonequilibrium lattice dynamics in PbSe QDs using UED experiments. Our results reveal the significant influence of oriented attachment on lattice dynamics. As shwon in Figure 5, along the attachment ⟨100⟩ directions, oriented attachment stiffens the lattice near {100} facets, leading to reduced expansion, diminished atom mean-square displacement, and accelerated relaxation kinetics. Conversely, along the ⟨111⟩ directions, oriented attachment induces an opposite trend. These insights provide valuable understanding of the anisotropic nanoscale energy flow pathways arising from oriented attachment, as well as nonradiative charge recombination mechanisms, crucial for optimizing QD-based device performance.

■ ASSOCIATED CONTENT

Supporting Information

The Supporting Information is available free of charge at https://pubs.acs.org/doi/10.1021/acs.jpclett.4c01541.

Descriptions of details of UED experiments and sample characterization, including absorbance spectra, TEM images and static expansion coefficient measurements of individual and attached QDs, the time-resolved Bragg peak width and intensity dynamics, lattice thermalization time constants from different Bragg peaks, and pump fluence-dependent lattice relaxation dynamics (PDF)

■ AUTHOR INFORMATION

Corresponding Authors

Chang Yan − *Center for Ultrafast Science and Technology, School of Chemistry and Chemical Engineering and Zhangjiang Institute for Advanced Study, Shanghai Jiao Tong University, Shanghai 200240, China;* orcid.org/0000-0001-9735-3002; Email: changyan@sjtu.edu.cn

Xuan Wang − *Beijing National Laboratory for Condensed Matter Physics, Institute of Physics, Chinese Academy of Sciences, Beijing 100190, China; Songshan Lake Materials Laboratory, Dongguan, Guangdong 523808, China;* Email: xw@iphy.ac.cn

Jianming Cao − *Physics Department and National High Magnetic Field Laboratory, Florida State University, Tallahassee, Florida 32310, United States; Center for Ultrafast Science and Technology, School of Physics and Astronomy, Shanghai Jiao Tong University, Shanghai 200240, China;* Email: jcao@magnet.fsu.edu

Authors

Luye Yue − *Center for Ultrafast Science and Technology, School of Physics and Astronomy, Shanghai Jiao Tong University, Shanghai 200240, China;* orcid.org/0000-0002-4483-108X

Jingjun Li − *Center for Ultrafast Science and Technology, School of Physics and Astronomy, Shanghai Jiao Tong University, Shanghai 200240, China*

Changyuan Yao − *Center for Ultrafast Science and Technology, School of Physics and Astronomy, Shanghai Jiao Tong University, Shanghai 200240, China*

Jie Chen − *Center for Ultrafast Science and Technology, School of Physics and Astronomy, Shanghai Jiao Tong University, Shanghai 200240, China;* orcid.org/0000-0001-5983-7479

Complete contact information is available at: https://pubs.acs.org/10.1021/acs.jpclett.4c01541

Notes

The authors declare no competing financial interest.

■ ACKNOWLEDGMENTS

The authors acknowledge Jianbing Zhang's group in the School of Optical and Electronic Information of Huazhong University of Science and Technology (HUST) in China for QD synthesis. This work is supported by the National Natural Science Foundation of China under Grants 11774409 and 11974241, the Youth Program of National Natural Science Foundation of China under Grant 11904394, the US-NSF Cooperative agreement (Grants DMR-1644779 and DMR-2128556), and the state of Florida. The authors also thank the UED experimental station under the Synergetic Extreme Condition User Facility (SECUF) in China.

■ REFERENCES

(1) Klimov, V. I.; Mikhailovsky, A. A.; Xu, S.; Malko, A.; Hollingsworth, J. A.; Leatherdale, C. A.; Eisler, H.-J.; Bawendi, M. G. Optical Gain and Stimulated Emission in Nanocrystal Quantum Dots. *Science* **2000**, *290* (5490), 314−317.

(2) Koleilat, G. I.; Levina, L.; Shukla, H.; Myrskog, S. H.; Hinds, S.; Pattantyus-Abraham, A. G.; Sargent, E. H. Efficient, Stable Infrared Photovoltaics Based on Solution-Cast Colloidal Quantum Dots. *ACS Nano* **2008**, *2* (5), 833−840.

(3) Talapin, D. V.; Lee, J. S.; Kovalenko, M. V.; Shevchenko, E. V. Prospects of Colloidal Nanocrystals for Electronic and Optoelectronic Applications. *Chem. Rev.* **2010**, *110* (1), 389−458.
(4) Kambhampati, P. Unraveling the Structure and Dynamics of Excitons in Semiconductor Quantum Dots. *Acc. Chem. Res.* **2011**, *44* (1), 1−13.
(5) Kovalenko, M. V.; Manna, L.; Cabot, A.; Hens, Z.; Talapin, D. V.; Kagan, C. R.; Klimov, V. I.; Rogach, A. L.; Reiss, P.; Milliron, D. J.; Guyot-Sionnnest, P.; Konstantatos, G.; Parak, W. J.; Hyeon, T.; Korgel, B. A.; Murray, C. B.; Heiss, W. Prospects of Nanoscience with Nanocrystals. *ACS Nano* **2015**, *9* (2), 1012−1057.
(6) Kagan, C. R.; Lifshitz, E.; Sargent, E. H.; Talapin, D. V. Building Devices from Colloidal Quantum Dots. *Science* **2016**, *353* (6302), aac5523.
(7) Garcia de Arquer, F. P.; Talapin, D. V.; Klimov, V. I.; Arakawa, Y.; Bayer, M.; Sargent, E. H. Semiconductor Quantum Dots: Technological Progress and Future Challenges. *Science* **2021**, *373* (6555), No. eaaz8541.
(8) Kagan, C. R.; Murray, C. B.; Bawendi, M. G. Long-Range Resonance Transfer of Electronic Excitations in Close-Packed CdSe Quantum-Dot Solids. *Phys. Rev. B* **1996**, *54* (12), 8633−8643.
(9) Sandeep, C. S. S.; Azpiroz, J. M.; Evers, W. H.; Boehme, S. C.; Moreels, I.; Kinge, S.; Siebbeles, L. D. A.; Infante, I.; Houtepen, A. J. Epitaxially Connected PbSe Quantum-Dot Films: Controlled Neck Formation and Optoelectronic Properties. *ACS Nano* **2014**, *8* (11), 11499−11511.
(10) Lan, X.; Chen, M.; Hudson, M. H.; Kamysbayev, V.; Wang, Y.; Guyot-Sionnest, P.; Talapin, D. V. Quantum Dot Solids Showing State-Resolved Band-like Transport. *Nat. Mater.* **2020**, *19* (3), 323−329.
(11) Ondry, J. C.; Alivisatos, A. P. Application of Dislocation Theory to Minimize Defects in Artificial Solids Built with Nanocrystal Building Blocks. *Acc. Chem. Res.* **2021**, *54* (6), 1419−1429.
(12) Koley, S.; Cui, J.; Panfil, Y. E.; Banin, U. Coupled Colloidal Quantum Dot Molecules. *Acc. Chem. Res.* **2021**, *54* (5), 1178−1188.
(13) Pinna, J.; Mehrabi Koushki, R.; Gavhane, D. S.; Ahmadi, M.; Mutalik, S.; Zohaib, M.; Protesescu, L.; Kooi, B. J.; Portale, G.; Loi, M. A. Approaching Bulk Mobility in PbSe Colloidal Quantum Dots 3D Superlattices. *Adv. Mater.* **2023**, *35* (8), 2207364.
(14) Kalesaki, E.; Delerue, C.; Morais Smith, C.; Beugeling, W.; Allan, G.; Vanmaekelbergh, D. Dirac Cones, Topological Edge States, and Nontrivial Flat Bands in Two-Dimensional Semiconductors with a Honeycomb Nanogeometry. *Phys. Rev. X* **2014**, *4* (1), 011010.
(15) Whitham, K.; Yang, J.; Savitzky, B. H.; Kourkoutis, L. F.; Wise, F.; Hanrath, T. Charge Transport and Localization in Atomically Coherent Quantum Dot Solids. *Nat. Mater.* **2016**, *15* (5), 557−563.
(16) Stern, M. J.; RenéDe Cotret, L. P.; Otto, M. R.; Chatelain, R. P.; Boisvert, J. P.; Sutton, M.; Siwick, B. J. Mapping Momentum-Dependent Electron-Phonon Coupling and Nonequilibrium Phonon Dynamics with Ultrafast Electron Diffuse Scattering. *Phys. Rev. B* **2018**, *97* (16), 1−7.
(17) René de Cotret, L. P.; Pöhls, J.-H.; Stern, M. J.; Otto, M. R.; Sutton, M.; Siwick, B. J. Time-and Momentum-Resolved Phonon Population Dynamics with Ultrafast Electron Diffuse Scattering. *Phys. Rev. B* **2019**, *100* (21), 214115.
(18) Dürr, H. A.; Ernstorfer, R.; Siwick, B. J. Revealing Momentum-Dependent Electron-Phonon and Phonon-Phonon Coupling in Complex Materials with Ultrafast Electron Diffuse Scattering. *MRS Bull.* **2021**, *46* (8), 731−737.
(19) Cooney, R. R.; Sewall, S. L.; Anderson, K. E. H.; Dias, E. A.; Kambhampati, P. Breaking the Phonon Bottleneck for Holes in Semiconductor Quantum Dots. *Phys. Rev. Lett.* **2007**, *98* (17), 1−4.
(20) Kambhampati, P. Hot Exciton Relaxation Dynamics in Semiconductor Quantum Dots: Radiationless Transitions on the Nanoscale. *J. Phys. Chem. C* **2011**, *115* (45), 22089−22109.
(21) Kaniyankandy, S.; Rawalekar, S.; Verma, S.; Palit, D. K.; Ghosh, H. N. Charge Carrier Dynamics in Thiol Capped CdTe Quantum Dots. *Phys. Chem. Chem. Phys.* **2010**, *12* (16), 4210−4216.
(22) Nootz, G.; Padilha, L. A.; Levina, L.; Sukhovatkin, V.; Webster, S.; Brzozowski, L.; Sargent, E. H.; Hagan, D. J.; Van Stryland, E. W. Size Dependence of Carrier Dynamics and Carrier Multiplication in PbS Quantum Dots. *Phys. Rev. B* **2011**, *83* (15), 155302.
(23) Bozyigit, D.; Yazdani, N.; Yarema, M.; Yarema, O.; Lin, W. M. M.; Volk, S.; Vuttivorakulchai, K.; Luisier, M.; Juranyi, F.; Wood, V. Soft Surfaces of Nanomaterials Enable Strong Phonon Interactions. *Nature* **2016**, *531* (7596), 618−622.
(24) Boneschanscher, M. P.; Evers, W. H.; Geuchies, J. J.; Altantzis, T.; Goris, B.; Rabouw, F. T.; van Rossum, S. A. P.; van der Zant, H. S. J.; Siebbeles, L. D. A.; Van Tendeloo, G.; Swart, I.; Hilhorst, J.; Petukhov, A. V.; Bals, S.; Vanmaekelbergh, D. Long-Range Orientation and Atomic Attachment of Nanocrystals in 2D Honeycomb Superlattices. *Science* **2014**, *344* (6190), 1377−1380.
(25) Wang, Y.; Peng, X.; Abelson, A.; Xiao, P.; Qian, C.; Yu, L.; Ophus, C.; Ercius, P.; Wang, L.-W.; Law, M.; Zheng, H. Dynamic Deformability of Individual PbSe Nanocrystals during Superlattice Phase Transitions. *Sci. Adv.* **2019**, *5* (6), No. eaaw5623.
(26) Ondry, J. C.; Philbin, J. P.; Lostica, M.; Rabani, E.; Alivisatos, A. P. Resilient Pathways to Atomic Attachment of Quantum Dot Dimers and Artificial Solids from Faceted CdSe Quantum Dot Building Blocks. *ACS Nano* **2019**, *13* (11), 12322−12344.
(27) Evers, W. H.; Schins, J. M.; Aerts, M.; Kulkarni, A.; Capiod, P.; Berthe, M.; Grandidier, B.; Delerue, C.; van der Zant, H. S. J.; van Overbeek, C.; Peters, J. L.; Vanmaekelbergh, D.; Siebbeles, L. D. A. High Charge Mobility in Two-Dimensional Percolative Networks of PbSe Quantum Dots Connected by Atomic Bonds. *Nat. Commun.* **2015**, *6* (1), 8195.
(28) Gilmore, R. H.; Liu, Y.; Shcherbakov-Wu, W.; Dahod, N. S.; Lee, E. M. Y.; Weidman, M. C.; Li, H.; Jean, J.; Bulović, V.; Willard, A. P.; Grossman, J. C.; Tisdale, W. A. Epitaxial Dimers and Auger-Assisted Detrapping in PbS Quantum Dot Solids. *Matter* **2019**, *1* (1), 250−265.
(29) Yan, C.; Weinberg, D.; Jasrasaria, D.; Kolaczkowski, M. A.; Liu, Z.-J.; Philbin, J. P.; Balan, A. D.; Liu, Y.; Schwartzberg, A. M.; Rabani, E.; Alivisatos, A. P. Uncovering the Role of Hole Traps in Promoting Hole Transfer from Multiexcitonic Quantum Dots to Molecular Acceptors. *ACS Nano* **2021**, *15* (2), 2281−2291.
(30) Zhang, Z.; Sung, J.; Toolan, D. T. W.; Han, S.; Pandya, R.; Weir, M. P.; Xiao, J.; Dowland, S.; Liu, M.; Ryan, A. J.; Jones, R. A. L.; Huang, S.; Rao, A. Ultrafast Exciton Transport at Early Times in Quantum Dot Solids. *Nat. Mater.* **2022**, *21* (5), 533−539.
(31) Yuan, R.; Roberts, T. D.; Brinn, R. M.; Choi, A. A.; Park, H. H.; Yan, C.; Ondry, J. C.; Khorasani, S.; Masiello, D. J.; Xu, K.; Alivisatos, A. P.; Ginsberg, N. S. A Composite Electrodynamic Mechanism to Reconcile Spatiotemporally Resolved Exciton Transport in Quantum Dot Superlattices. *Sci. Adv.* **2023**, *9* (42), No. eadh2410.
(32) Sewall, S. L.; Cooney, R. R.; Anderson, K. E. H.; Dias, E. A.; Sagar, D. M.; Kambhampati, P. State-Resolved Studies of Biexcitons and Surface Trapping Dynamics in Semiconductor Quantum Dots. *J. Chem. Phys.* **2008**, *129* (8), 084701.
(33) Mooney, J.; Krause, M. M.; Saari, J. I.; Kambhampati, P. Challenge to the Deep-Trap Model of the Surface in Semiconductor Nanocrystals. *Phys. Rev. B* **2013**, *87* (8), 081201.
(34) Kambhampati, P. On the Kinetics and Thermodynamics of Excitons at the Surface of Semiconductor Nanocrystals: Are There Surface Excitons? *Chem. Phys.* **2015**, *446*, 92−107.
(35) Jethi, L.; Mack, T. G.; Kambhampati, P. Extending Semiconductor Nanocrystals from the Quantum Dot Regime to the Molecular Cluster Regime. *J. Phys. Chem. C* **2017**, *121* (46), 26102−26107.
(36) Tao, Z.; Zhou, F.; Han, T. R. T.; Torres, D.; Wang, T.; Sepulveda, N.; Chang, K.; Young, M.; Lunt, R. R.; Ruan, C. Y. The Nature of Photoinduced Phase Transition and Metastable States in Vanadium Dioxide. *Sci. Rep.* **2016**, *6* (1), 38514.
(37) Zhou, F.; Williams, J.; Sun, S.; Malliakas, C. D.; Kanatzidis, M. G.; Kemper, A. F.; Ruan, C. Y. Nonequilibrium Dynamics of Spontaneous Symmetry Breaking into a Hidden State of Charge-Density Wave. *Nat. Commun.* **2021**, *12* (1), 566.

https://doi.org/10.1021/acs.jpclett.4c01541
J. Phys. Chem. Lett. 2024, 15, 7667−7673

(38) Chebl, M.; He, X.; Yang, D.-S. Ultrafast Carrier-Coupled Interlayer Contraction, Coherent Intralayer Motions, and Phonon Thermalization Dynamics of Black Phosphorus. *Nano Lett.* **2022**, *22* (13), 5230−5235.
(39) Li, J.; Wu, L.; Yang, S.; Jin, X.; Wang, W.; Tao, J.; Boatner, L.; Babzien, M.; Fedurin, M.; Palmer, M.; Yin, W.; Delaire, O.; Zhu, Y. Direct Detection of V-V Atom Dimerization and Rotation Dynamic Pathways upon Ultrafast Photoexcitation in VO2. *Phys. Rev. X* **2022**, *12* (2), 21032.
(40) Zhang, H.; Li, W.; Essman, J.; Quarti, C.; Metcalf, I.; Chiang, W.-Y.; Sidhik, S.; Hou, J.; Fehr, A.; Attar, A.; et al. Ultrafast Relaxation of Lattice Distortion in Two-Dimensional Perovskites. *Nat. Phys.* **2023**, *19* (4), 545−550.
(41) Vanacore, G. M.; Hu, J.; Liang, W.; Bietti, S.; Sanguinetti, S.; Zewail, A. H. Diffraction of Quantum Dots Reveals Nanoscale Ultrafast Energy Localization. *Nano Lett.* **2014**, *14* (11), 6148−6154.
(42) Wang, X.; Rahmani, H.; Zhou, J.; Gorfien, M.; Mendez Plaskus, J.; Li, D.; Voss, R.; Nelson, C. A.; Wai Lei, K.; Wolcott, A.; Zhu, X.; Li, J.; Cao, J. Ultrafast Lattice Dynamics in Lead Selenide Quantum Dot Induced by Laser Excitation. *Appl. Phys. Lett.* **2016**, *109* (15), 153105.
(43) Vasileiadis, T.; Waldecker, L.; Foster, D.; Da Silva, A.; Zahn, D.; Bertoni, R.; Palmer, R. E.; Ernstorfer, R. Ultrafast Heat Flow in Heterostructures of Au Nanoclusters on Thin Films: Atomic Disorder Induced by Hot Electrons. *ACS Nano* **2018**, *12* (8), 7710−7720.
(44) Seiler, H.; Zahn, D.; Taylor, V. C.; Bodnarchuk, M. I.; Windsor, Y. W.; Kovalenko, M. V.; Ernstorfer, R. Direct Observation of Ultrafast Lattice Distortions during Exciton-Polaron Formation in Lead Halide Perovskite Nanocrystals. *ACS Nano* **2023**, *17* (3), 1979−1988.
(45) Guzelturk, B.; Cotts, B. L.; Jasrasaria, D.; Philbin, J. P.; Hanifi, D. A.; Koscher, B. A.; Balan, A. D.; Curling, E.; Zajac, M.; Park, S.; Yazdani, N.; Nyby, C.; Kamysbayev, V.; Fischer, S.; Nett, Z.; Shen, X.; Kozina, M. E.; Lin, M.-F.; Reid, A. H.; Weathersby, S. P.; Schaller, R. D.; Wood, V.; Wang, X.; Dionne, J. A.; Talapin, D. V.; Alivisatos, A. P.; Salleo, A.; Rabani, E.; Lindenberg, A. M. Dynamic Lattice Distortions Driven by Surface Trapping in Semiconductor Nanocrystals. *Nat. Commun.* **2021**, *12* (1), 1860.
(46) Krawczyk, K. M.; Sarracini, A.; Green, P. B.; Hasham, M.; Tang, K.; Paré-Labrosse, O.; Voznyy, O.; Wilson, M. W. B.; Miller, R. J. D. Anisotropic, Nonthermal Lattice Disordering Observed in Photoexcited PbS Quantum Dots. *J. Phys. Chem. C* **2021**, *125* (40), 22120−22132.
(47) Guzelturk, B.; Lindenberg, A. M.; Utterback, J. K.; Coropceanu, I.; Kamysbayev, V.; Janke, E. M.; Zajac, M.; Yazdani, N.; Cotts, B. L.; Park, S.; Sood, A.; Lin, M. F.; Reid, A. H.; Kozina, M. E.; Shen, X.; Weathersby, S. P.; Wood, V.; Salleo, A.; Wang, X.; Talapin, D. V.; Ginsberg, N. S. Nonequilibrium Thermodynamics of Colloidal Gold Nanocrystals Monitored by Ultrafast Electron Diffraction and Optical Scattering Microscopy. *ACS Nano* **2020**, *14* (4), 4792−4804.
(48) Zhang, J.; Gao, J.; Miller, E. M.; Luther, J. M.; Beard, M. C. Diffusion-Controlled Synthesis of PbS and PbSe Quantum Dots with in Situ Halide Passivation for Quantum Dot Solar Cells. *ACS Nano* **2014**, *8* (1), 614−622.
(49) Lian, L.; Xia, Y.; Zhang, C.; Xu, B.; Yang, L.; Liu, H.; Zhang, D.; Wang, K.; Gao, J.; Zhang, J. In Situ Tuning the Reactivity of Selenium Precursor to Synthesize Wide Range Size, Ultralarge-Scale, and Ultrastable PbSe Quantum Dots. *Chem. Mater.* **2018**, *30* (3), 982−989.
(50) Choi, H.; Ko, J.-H.; Kim, Y.-H.; Jeong, S. Steric-Hindrance-Driven Shape Transition in PbS Quantum Dots: Understanding Size-Dependent Stability. *J. Am. Chem. Soc.* **2013**, *135* (14), 5278−5281.
(51) Hughes, B. K.; Ruddy, D. A.; Blackburn, J. L.; Smith, D. K.; Bergren, M. R.; Nozik, A. J.; Johnson, J. C.; Beard, M. C. Control of PbSe Quantum Dot Surface Chemistry and Photophysics Using an Alkylselenide Ligand. *ACS Nano* **2012**, *6* (6), 5498−5506.
(52) Wang, Y.; Peng, X.; Abelson, A.; Zhang, B.-K.; Qian, C.; Ercius, P.; Wang, L.-W.; Law, M.; Zheng, H. In Situ TEM Observation of Neck Formation during Oriented Attachment of PbSe Nanocrystals. *Nano Res.* **2019**, *12* (10), 2549−2553.
(53) Choi, J. J.; Bealing, C. R.; Bian, K.; Hughes, K. J.; Zhang, W.; Smilgies, D.-M.; Hennig, R. G.; Engstrom, J. R.; Hanrath, T. Controlling Nanocrystal Superlattice Symmetry and Shape-Anisotropic Interactions through Variable Ligand Surface Coverage. *J. Am. Chem. Soc.* **2011**, *133* (9), 3131−3138.
(54) Bealing, C. R.; Baumgardner, W. J.; Choi, J. J.; Hanrath, T.; Hennig, R. G. Predicting Nanocrystal Shape through Consideration of Surface-Ligand Interactions. *ACS Nano* **2012**, *6* (3), 2118−2127.
(55) Baumgardner, W. J.; Whitham, K.; Hanrath, T. Confined-but-Connected Quantum Solids via Controlled Ligand Displacement. *Nano Lett.* **2013**, *13* (7), 3225−3231.
(56) Cho, K. S.; Talapin, D. V.; Gaschler, W.; Murray, C. B. Designing PbSe Nanowires and Nanorings through Oriented Attachment of Nanoparticles. *J. Am. Chem. Soc.* **2005**, *127* (19), 7140−7147.
(57) Ondry, J. C.; Hauwiller, M. R.; Alivisatos, A. P. Dynamics and Removal Pathway of Edge Dislocations in Imperfectly Attached PbTe Nanocrystal Pairs: Toward Design Rules for Oriented Attachment. *ACS Nano* **2018**, *12* (4), 3178−3189.
(58) Yue, L.; Li, J.; Qi, Y.; Chen, J.; Wang, X.; Cao, J. Auger Recombination and Carrier-Lattice Thermalization in Semiconductor Quantum Dots under Intense Excitation. *Nano Lett.* **2023**, *23* (7), 2578−2585.
(59) El-Ballouli, A. O.; Alarousu, E.; Usman, A.; Pan, J.; Bakr, O. M.; Mohammed, O. F. Real-Time Observation of Ultrafast Intraband Relaxation and Exciton Multiplication in PbS Quantum Dots. *ACS Photonics* **2014**, *1* (3), 285−292.
(60) Barrera, G. D.; Bruno, J. A. O.; Barron, T.; Allan, N. Negative Thermal Expansion. *J. Phys.: Condens. Matter* **2005**, *17* (4), R217.
(61) Boles, M. A.; Ling, D.; Hyeon, T.; Talapin, D. V. The Surface Science of Nanocrystals. *Nat. Mater.* **2016**, *15* (2), 141−153.
(62) Argeri, M.; Fraccarollo, A.; Grassi, F.; Marchese, L.; Cossi, M. Density Functional Theory Modeling of PbSe Nanoclusters: Effect of Surface Passivation on Shape and Composition. *J. Phys. Chem. C* **2011**, *115*, 11382−11389.
(63) Yazdani, N.; Bozyigit, D.; Vuttivorakulchai, K.; Luisier, M.; Infante, I.; Wood, V. Tuning Electron-Phonon Interactions in Nanocrystals through Surface Termination. *Nano Lett.* **2018**, *18* (4), 2233−2242.
(64) Yang, D. S.; Gedik, N.; Zewail, A. H. Ultrafast Electron Crystallography. 1. Nonequilibrium Dynamics of Nanometer-Scale Structures. *J. Phys. Chem. C* **2007**, *111* (13), 4889−4919.
(65) Lee, J.-S.; Kovalenko, M. V.; Huang, J.; Chung, D. S.; Talapin, D. V. Band-like Transport, High Electron Mobility and High Photoconductivity in All-Inorganic Nanocrystal Arrays. *Nat. Nanotechnol.* **2011**, *6* (6), 348−352.
(66) Gao, Y.; Talgorn, E.; Aerts, M.; Trinh, M. T.; Schins, J. M.; Houtepen, A. J.; Siebbeles, L. D. A. Enhanced Hot-Carrier Cooling and Ultrafast Spectral Diffusion in Strongly Coupled PbSe Quantum-Dot Solids. *Nano Lett.* **2011**, *11* (12), 5471−5476.
(67) Kim, D.; Kim, D.-H.; Lee, J.-H.; Grossman, J. C. Impact of Stoichiometry on the Electronic Structure of PbS Quantum Dots. *Phys. Rev. Lett.* **2013**, *110* (19), 196802.
(68) Bian, K.; Bassett, W.; Wang, Z.; Hanrath, T. The Strongest Particle: Size-Dependent Elastic Strength and Debye Temperature of PbS Nanocrystals. *J. Phys. Chem. Lett.* **2014**, *5* (21), 3688−3693.

https://doi.org/10.1021/acs.jpclett.4c01541
J. Phys. Chem. Lett. 2024, 15, 7667−7673